University of Guilan

Caspian Journal of Intelligent and Mechatronic Systems

https://cjiams.guilan.ac.ir

Caspian Journal of INTELLIGENT and MECHATRONIC SYSTEM

Practice Article

Digital Twin-Based Performance Prediction and Operational Constraint Management in SGT5-2000E / MGT-70(3) Gas Turbines

Amirreza Mostafavi [a,c], Farzad Farokhi [a], Ali Chaibakhsh [b,c,*]

[a.] *MAPNA Power Services Company, Tehran Province, Iran*

[b.] *Faculty of Mechanical Engineering, University of Guilan, Rasht, Guilan, Iran*

[c.] *Intelligent Systems and Advanced Control Lab., University of Guilan, Rasht, Guilan, Iran*

ARTICLE INFO

Article history:
Received October 8, 2026
Accepted November 17, 2026
Available online November 17, 2026

Keywords
Heat rate degradation
Mass flow rate
Ambient condition sensitivity
Climate changes
Thermodynamic simulation
Empirical correlations
Derating

ABSTRACT

Heavy-duty industrial gas turbines operating in high-altitude and arid environments can experience substantial performance degradation and efficiency losses. This study develops an operationally oriented thermodynamic and correction-factor framework for the 183 MW SGT5-2000E / MGT-70(3) gas turbine to evaluate performance under site-specific conditions. A comprehensive off-design model was applied to examine the effects of relative humidity, barometric pressure, compressor inlet temperature, and fuel properties. Using one year of operating data, the site's ambient-pressure conditions, and a digital-twin model, operational correction charts were regenerated for the turbine's actual operating envelope, rather than for its entire nominal range. The results show that sub-atmospheric site pressure and inlet pressure losses of 13.8 ~ 21.1 mbar combine to reduce available power, with annual generation remaining below 80% of nominal capacity. Piecewise quadratic regressions were developed to represent performance variations near operational limits at low compressor inlet temperatures, together with bounding formulations for changes in fuel quality. The resulting correlations and site-specific charts provide a basis for estimating power output, air mass flow, thermal efficiency, and exhaust temperature across the operating conditions observed at the installation site.

*. Corresponding author. Tel.: +98-13-33691065; Fax: +98-13-33691065.
E-mail address: chaibakhsh@guilan.ac.ir; chaibakhsh@gmail.com (A. Chaibakhsh).

Doi:10.22124/cjiams.2026.35683.1002

© 2026 Published by University of Guilan

Proofed

1. Introduction

Gas turbines are critical assets in global power generation. Their operational efficacy is intrinsically linked to the thermodynamic state of the intake air, as atmospheric conditions dictate both the working fluid mass flow and the cycle's specific work. operating environments frequently diverge significantly from these standard ratings, leading to distinct off-design performance behaviors [1, 2].

A significant challenge in plant asset management is the reliance on simplistic correction factors, which frequently operate under the assumption that ambient parameters, temperature, pressure, and humidity, affect turbine performance independently. In practice, these variables are coupled; environmental shifts, such as daytime temperature swings in arid regions, simultaneously alter air density, compression requirements, and the thermodynamic properties of the gas path. Furthermore, the mechanistic impact of these variables is non-uniform: temperature acts primarily on density and compressor work, whereas humidity alters the polytropic compression exponent and heat transfer characteristics. Consequently, applying universal correction factors to site-specific conditions without calibration often introduces systematic errors in dispatch planning and performance verification [3, 4].

Furthermore, because industrial gas turbines operating in severe arid environments frequently run at off-design points, often generating up to 20% below their nominal ISO capacity, relying solely on generic experimental data or simplistic correction curves becomes inadequate. Such empirical datasets rarely cover the full operational envelope or capture unpredicted off-design extremes. To overcome this limitation, correction factors must either be established through rigorous point-by-point interpolation or derived via a calibrated physics-based digital twin model [5, 6]. Once aligned with baseline ISO specifications, this model systematically maps performance variations across wide ambient temperature, pressure, and humidity ranges, yielding high-fidelity correction functions that outperform conventional, decoupled static charts [7, 8].

This technical note addresses these challenges by replacing computationally intensive iterative cycle solvers with explicit, climate-calibrated empirical correlations. The objective is to provide a reliable and real-time framework to compute derated mass flow and expected power output without the overhead of complex numerical solvers. While operational correction curves are formulated as individual functions of temperature, pressure, and humidity, combined multiplicatively for dispatch evaluation, they are derived directly from systematic sensitivity sweeps of a multi-variable, physics-based digital twin. To this end, a site-specific digital twin of the SGT5-2000E / MGT-70(3) unit was calibrated against 9,299 archived ambient records, covering ambient temperatures from -1 to 43.1 ^{o}C, sub-atmospheric pressures from 80.1 to 87.4 kPa and relative humidity ranging from below 15% (typical) to 95% (maximum). This calibrated digital twin serves as the reference engine for systematic sensitivity sweeps, following the digital-twin paradigm, in which a virtual duplication benchmarks expected output and key performance variables against real-time plant data.

PROOF Read

Nomenclature

c	Specific heat	(kJ/kg K)
e	Exponential function (exp)	-
E^*	Effendy correction factor	
K	Coefficient	-
L	Delay	(s)
M	Mach number	(kg)
M^*	Mass correction factor	
$\dot{m}$	Mass flow	(kg/s)
n	Flow exponent	-
N	Normal / Natural	-
p	Pressure	-
P^*	Power correction factor	(kPa)
Q	Heat transferred	(kJ)
q	Flow rate	(m^3/s)
$\dot{Q}$	Heat rate	(W)
R	Valve rangeability	-
s	Laplace	-
t	Time	(s)
T	Temperature	(ºC) / (K)
$\bar{T}$	Temperature Average	(ºC) / (K)
T^*	Temperature correction factor	-
$\dot{W}$	Power	(MW)
x / X	Variable / Correction Factor	
z	Compressibility factor	-
A/F	Air-fuel ratio	-
CPR	Compressor pressure ratio	-
H/C	Hydrogen - Carbon	
HP	High pressure	-
IGV	Inlet guide vane	-
ISO	ISO standard conditions	
LHV	Low heat valve	(MJ/kg)
MCV	Main control valve	-
OEM	Original equipment manufacturer	
OTC	Outlet temperature corrected	(K)
PID	PID controller	-
RH	Relative humidity	%
TET	Exhaust gas temperature	(K)

Subscripts

air	Air
amb	Ambient
base	Base
comb	Combustion
comp	Compressor
corrected	Corrected value
cpr	Compressor pressure ratio
dis	Discharge
Δp	Differential pressure
e	Electrical
eff	Efficiency
exhst	Exhaust
filters	Filter
gen	Generated value / Generator
igv	Inlet guide vane
in	Input / Inlet
intake	Intake air duct
iso	ISO conditions
N	Normal conditions
out	Output
p	Constant pressure
span	Span
temp	Temperature
total	Total
turb	Turbine
0	Initial value / Standard condition

Greek letters

Δ	Differential	-
γ	The specific heats ratio	-
Γ	Torque	(N.m)
δ	Correction factor	-
η	Efficiency	(%)
θ	Angle	-
υ	Constant volume	-
ρ	Specific density	(kg/m^3)
τ	Time constant	(s)
χ	IGV position	(%)
ω	Frequency	(rad/s)

Proof Read

By examining the digital twin over a wide range of operation of site and fuel conditions, key performance correction factors are extracted directly from the model rather than relying on generic curves. This methodology aligns with recent digital twin frameworks focused on gas turbine thermodynamic modeling and real-time performance optimization. Finally, the correlations derived from the digital twin are compiled into operator-ready correction tables and standard correction charts, enabling the real-time conversion of ambient-condition and fuel-quality measurements into nominal power setpoints and corresponding fuel schedules.

The remainder of this technical note presents the model-calibration procedure, details the extraction of each correction family, and validates the resulting tables and charts against measured transient and steady-state data.

2. Gas Turbine Unit

The Siemens SGT5-2000E heavy-duty gas turbine, historically designated the V94.2 and localized within the MAPNA Turbine Engineering & Manufacturing Co. (TUGA) as the MGT-70, is among the most widely deployed single-shaft prime movers in the 50 Hz market [9]. More than 315 units have been sold, accumulating over 33 million equivalent operating hours with a fleet reliability consistently exceeding 99.5 percent. In the competitive power-generation landscape, capital and operational cost, mechanical durability, and operational flexibility are the primary criteria for plant asset management, and the SGT5-2000E addresses all three through manufacturing robustness, high availability in both simple-cycle and combined-cycle configurations, and an exceptionally broad fuel envelope [9, 10].

Under standard ISO rating conditions (T_{amb} = 15 °C, p_{amb} = 1.013 bar, RH = 60 %), the OEM specifies the following gross performance data for 183-MW SGT5-2000E / MGT-70(3) are as follows [11],

- Gross electrical power output: 183.0 MW
- Gross thermal efficiency: 36.4%
- Nominal shaft speed: 3000 rpm (50 Hz grid)
- Compressor pressure ratio: 12.0:1
- Exhaust flue-gas mass flow: 554.0 kg/s
- Exhaust gas temperature: 544.0 °C

The core turbomachine comprises a 16-stage axial-flow compressor with variable-pitch inlet guide vanes (VIGVs) and a 4-stage axial turbine mounted on a single-piece, dual-bearing rotor. This architecture is the subject of the present note, which concerns how much of the rated 183 MW survives when the machine operates far from the ISO reference point. Table 1 consolidates the baseline specifications drawn from the OEM datasheet and the plant rating documentation [11].

Table 1. Baseline nominal specifications of the 183-MW MGT-70(3) gas turbine under ISO conditions [11].

No.	Parameter	Unit	Value
1	Gross power output*	MW	183.0
2	Gross efficiency*	%	36.4
3	Shaft speed	rpm	3000
4	Exhaust gas temperature (*TET*)	°C	544.0
5	Exhaust mass flow rate	kg/s	554.0
6	Number of compressor stages	—	16
7	Number of turbine stages	—	4
8	Compressor pressure ratio (*CPR*)	—	12.0
9	Combustor type	—	Silo type (dual)
10	NO_x emissions	ppmvd @ 15% O_2	25
11	CO emissions	ppmvd @ 15% O_2	10
12	Grid frequency	Hz	50

Proof Read

2. Operating conditions

Gas turbines are highly sensitive to variations in ambient conditions and regional meteorological profiles. Consequently, meticulous site selection and environmental assessment are crucial during the preliminary design phase. Operating in extreme climates, characterized by elevated ambient temperatures, low barometric pressures, severe relative humidity extremes, and high dust or sandstorm loading, can induce severe performance degradation and capacity loss unless properly mitigated [12, 13].

This is particularly relevant to the gas turbine considered in this study, which operates at a site where the measured ambient temperature ranges from -1 to 43 °C and the barometric pressure varies from 80.1 to 87.4 kPa (mean approximately 82.5 kPa), substantially below the ISO reference pressure of 101.325 kPa. The site's low pressure reduces inlet-air density and therefore the available turbine power; the magnitude of the reduction also depends on ambient temperature and relative humidity.

Accordingly, the power correction factor must be evaluated using the combined site conditions rather than temperature alone [14]. As it is illustrated in Figure 1, the annual generated power profile of Unit #1 over the one-year operational period highlights the maximum, minimum, and baseline performance levels. As demonstrated by the temporal variations, due to the severe site-specific environmental conditions, particularly the low ambient barometric pressures, the turbine's actual power output remains constrained, never exceeding 80 percent of its nominal capacity throughout the entire annual cycle.

In Figure 2, the power correction factor (P^*) versus relative humidity (RH) is presented, in which with all isotherms converging at the RH=60% reference point (P^*=1.000). Over the temperature range shown, the humidity effect is temperature-dependent: the curves exhibit a relatively mild variation at moderate temperatures, while the high-temperature curves show stronger nonlinear behavior. This behavior is consistent with the increase in water-vapor partial pressure with temperature and the consequent displacement of part of the dry-air mixture.

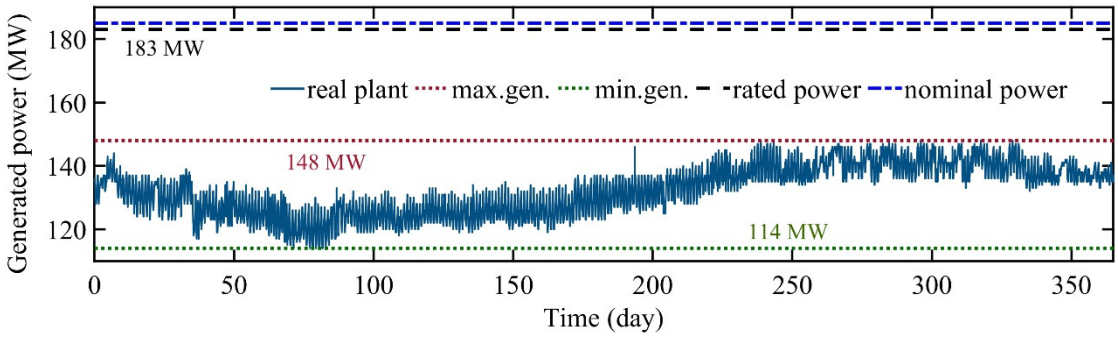


Figure 1. Annual generated power profile of Unit #1 over a one-year operational period, illustrating the maximum, minimum, and baseline/nominal power outputs

PROOF

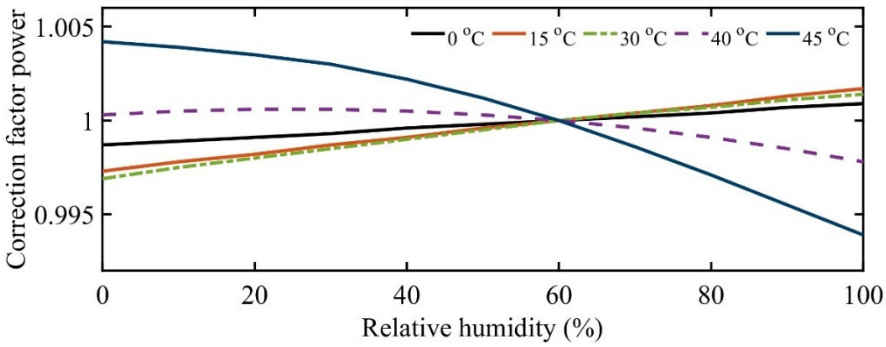


Figure 2. Effect of ambient relative humidity on the correction factor of generated power.

At a given vapor partial pressure, the lower site barometric pressure increases the vapor mole fraction, $y_v = p_v / P_{amb}$, and can therefore amplify the relative influence of moisture. The measured site data cover -1 to 43 °C; consequently, correction factors within this interval should be evaluated using the measured ambient pressure and relative humidity, with interpolation were justified by the available performance data.

The plotted isotherms at temperatures outside the measured range, particularly the 45 °C curve, do not represent observed operating conditions at this site and should not be treated as validated site-specific corrections. Extrapolation beyond the available temperature range is not recommended without additional manufacturer performance data or a validated thermodynamic model that accounts for the coupled effects of ambient temperature, pressure, and humidity. For performance assessment, the applicable gas-turbine test and acceptance standards, such as ISO 2314 or ASME PTC 22, should be followed [15, 16].

In Figure 3, the effect of ambient temperature on the correction factors for the power and efficiency are presented. While static lookup tables and 1-D empirical curves, such as the power (P^*) and efficiency (η^*) derating trends depicted above, as baselines relative to ISO conditions (15 °C), they prove inadequate in environments with severe daytime temperature swings, such as desert climates.

Under ISO reference conditions, a reduction in ambient temperature may suggest that higher power capacities are achievable due to increased air density and compressor mass flow. However, the actual output is strictly bounded by the turbine's mechanical and structural limits. For the unit under consideration, given that the site barometric pressure is significantly below standard atmospheric levels, reaching such elevated capacities is further restricted by operational constraints. As discussed in the following sections, at low ambient temperatures, the control system limits the output through the corrected turbine outlet temperature (OTC) logic, preventing the turbine from exceeding its operating restrictions.

3. Gas Path Modelling

Considering that operational conditions at power plant sites, particularly in hot and arid climates, consistently deviate from standard ISO conditions, accurate performance analysis based solely on field monitoring data is challenging. To address this, the optimal approach is to develop

Proof Read

a baseline analytical model grounded in the MGT-70 turbine's nominal specifications at the design point. Defining these reference parameters precisely establishes a robust framework for calculating performance deviations and predicting machine behavior under actual operating conditions.

Simcenter™ Amesim provides a specialized platform for modeling gas turbine systems, facilitating accurate simulation of the gas path and thermal interactions. Using a single-shaft configuration, the MGT-70(3) turbine structure is partitioned into separate stations, including the air inlet, compressor, combustion chamber, and turbine section. Operational parameters such as pressure, temperature, and mass flow rate are initialized at each station using nominal ISO design-point data, enabling the software to model individual components and establish the system energy balance. This modular structure enhances calibration and simulation fidelity over global numerical approaches. Figure 4 illustrates the considered stations and design-point parameters.

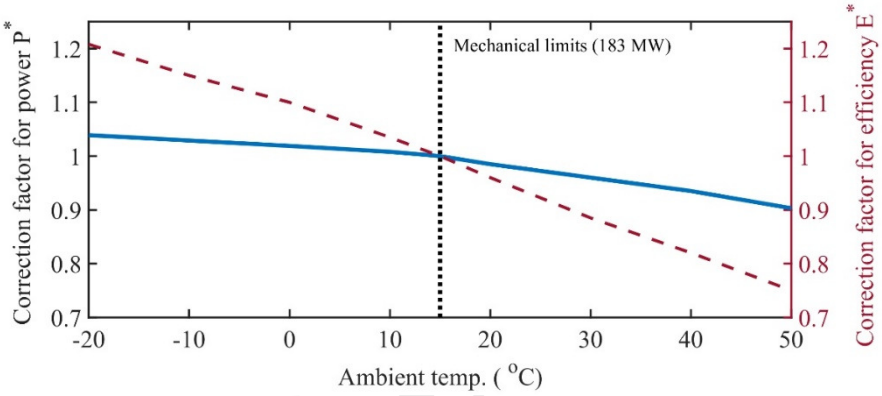
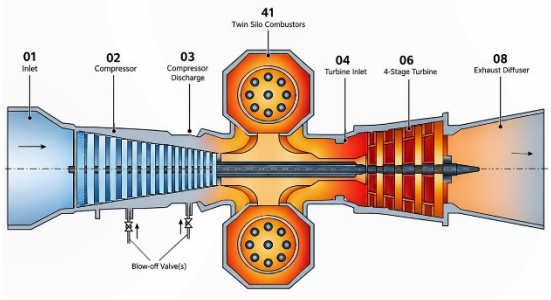


Figure 3. Effect of ambient temperature on the correction factors for the power and efficiency.



Station 01		
Parameter	Value	Unit
Total pressure*	103.0326	kPa
Total temperature	288.15	K
Ambient pressure	101.325	kPa
Relative humidity	60	%
Mach number*	0.1547	-

*. Total pressure is calculated from the ambient pressure and the Mach number of the flow in the air-intake duct

Station 02		
Parameter	Value	Unit
Inlet corrected mass flow rate	560	kg/s
Intake pressure ratio	0.98	-
Mach number	0.5	-

Station 03		
Parameter	Value	Unit
HPC pressure ratio	12	-
HPC isentropic efficiency	0.88	-
High pressure shaft rotary speed	3000	rpm
HPC shaft mechanical power efficiency	1	-
Mach number	0.45	-

Station 41		
Parameter	Value	Unit
Burner exit temperature	1403.15	K
Burner efficiency	0.999	-
Burner pressure ratio	0.98	-
Fuel / Air ratio	0.023	-
Fuel LHV	48.594	MJ/kg
Mach number	0.43	-

Station 04		
Parameter	Value	Unit
Temperature	1205	K
Mach number	0.5	-

Station 06		
Parameter	Value	Unit
HPT isentropic efficiency	0.90	-
Mach number	0.43	-

Station 08		
Parameter	Value	Unit
Exhaust pressure ratio	1.04	-

Figure 4. Schematic layout and corresponding operating station parameters of the SGT5-2000E gas turbine model implemented in Amesim, illustrating thermodynamic states from ambient inlet (Station 01) to exhaust (Station 08).

To ensure that component efficiency is mapped independently of atmospheric variables, the operational data is transformed into a corrected presentation, effectively filtering out the influence of changing environmental conditions. The corrected mass flow rate and corrected rotor speed are defined as follows,

Corrected mass flow rate: $$\dot{m}_{corrected} = \dot{m}\,\frac{p_{iso}}{p}\sqrt{\frac{T}{T_{iso}}} \quad (1)$$

Corrected rotor speed: $$\omega_{corrected} = \omega\sqrt{\frac{T_{iso}}{T}} \quad (2)$$

Once the model is established at the design point, simulations are executed across varying operating points to extract performance maps for critical components, specifically the compressor and turbine. Compressor maps are generated by plotting the compressor pressure ratio (PR) against corrected mass flow, while turbine maps are based on corrected mass flow × normalized rotational speed versus pressure ratio of the turbine. These maps characterize the machine's operational behaviors across various working conditions.

Figure 5 illustrates the performance maps of the primary SGT5-2000E gas turbine components: the compressor (a) and the turbine (b). These maps provide critical insights into component behavior and efficiency across diverse operational envelopes, ranging from rated design points to off-design scenarios. Figure 5-a presents the compressor performance map, characterized by distinct operating trajectories. These paths delineate the compressor's response across various engine phases, including startup, acceleration, steady-state operation, and deceleration. Analyzing these trajectories is essential for evaluating compressor stability, validating control strategies, and monitoring operational safety margins relative to the surge line. In Figure 5-b, the performance map for the turbine section is presented. By plotting the corrected mass flow rate (normalized by rotational speed) against the pressure ratio, this map defines the turbine's operational limits. These operational trajectories allow for a detailed assessment of turbine behavior across different regimes, highlighting how the component adapts to varying power demands and environmental conditions.

The primary outcome of this modeling approach is the ability to analyze turbine performance under off-design conditions. By employing the compressor and turbine maps and incorporating precise component sizing data (such as polytropic efficiencies, pressure ratios, and load-dependent characteristics), the model can accurately predict system behavior in response to fluctuating environmental conditions.

Although key performance indicators, such as net power output, thermal efficiency, core mass flow rate, and exhaust gas temperature, are theoretically expected to be direct functions of ambient boundary conditions (temperature, pressure, and relative humidity), directly extracting them from multidimensional compressor and turbine maps remains computationally demanding.

Proof Read

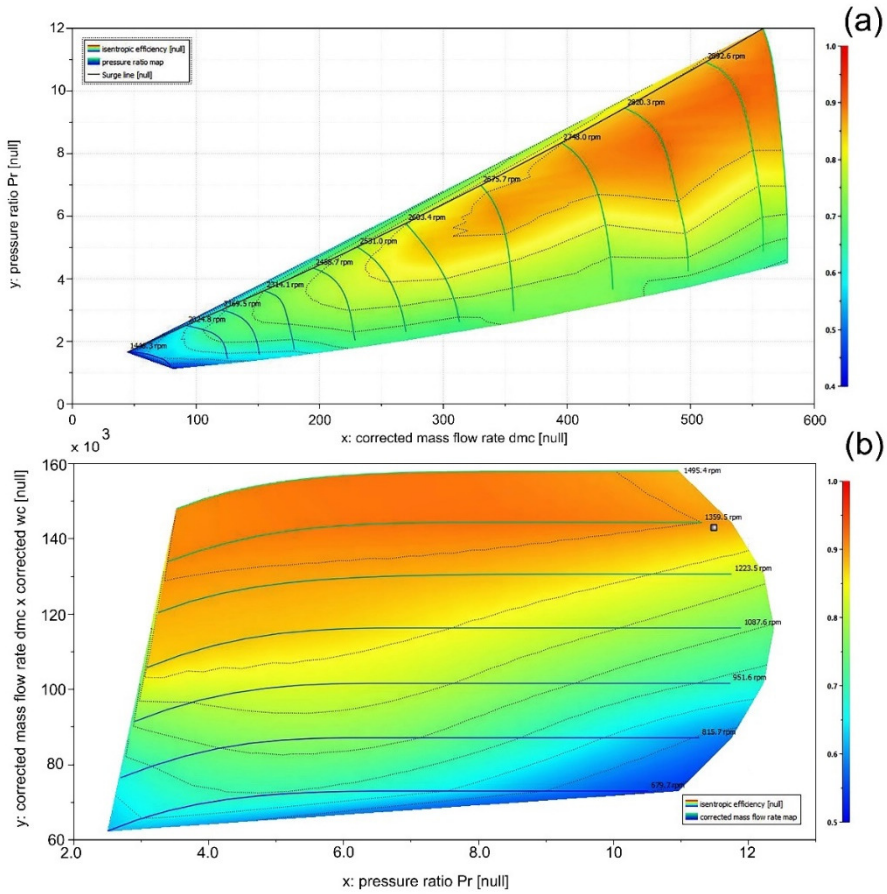


Figure 5. Performance maps with operating point trajectories of the SGT5-2000E components: (a) Compressor section map; (b) Turbine section map

Consequently, original equipment manufacturers (OEMs) have traditionally relied on linear correction factors and empirical performance curves within operation manuals and acceptance test codes. These correction tools remain vital for plant operators in day-ahead scheduling, generation dispatching, and seasonal off-design forecasting.

The emergence of digital twin architectures is progressively replacing these conventional simplified correlations. By developing a sophisticated thermodynamic toolbox, the non-linear coupling of the gas turbine cycle can be resolved with high fidelity, enabling the precise estimation of aerodynamic mass flow rates, fuel demand, and component-level efficiencies across the entire operating envelope.

By extracting and validating the compressor and turbine characteristic maps and integrating them into a high-fidelity thermodynamic model, a computational framework was established to fully capture coupled environmental effects under extreme operating regimes. This framework not only reveals and rectifies the inherent discrepancies of OEM empirical correlations, but also functions as a lightweight digital twin, enabling plant operators to continuously estimate unmeasured aerodynamic and combustion variables. Accordingly, based on the thermodynamic model proposed by Chaibakhsh and Amirkhani [9], the governing equations of the various engine subcomponents, most notably the axial compressor, can be systematically implemented to resolve the core aerodynamic mass flow rate and comprehensively analyze the gas turbine behavior.

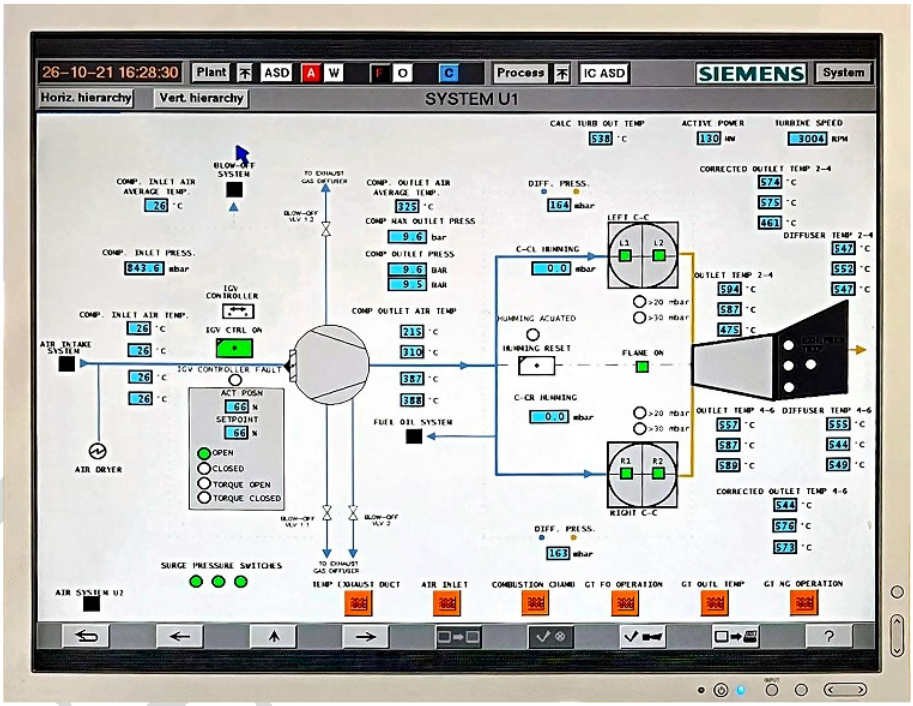


Figure 6. SCADA system and monitoring interface of the SGT5-2000E gas turbine unit

Adopting such a high-fidelity analytical model is particularly advantageous because it rigorously captures multi-dimensional, non-linear aerothermodynamic phenomena, including internal pressure drops, variable inlet guide vane (IGV) kinematics, bleed air extractions, and ambient-induced density variations through coupled mass and energy conservation, which remain inherently inaccessible via conventional empirical approximations.

The measured steady-state characteristics and transient trajectories provide the experimental basis for calibrating the gas-turbine model. In particular, the time-dependent responses of the recorded variables are used to estimate the model's dynamic parameters, including relevant time constants and delays. As illustrated in Figure 6, the plant's SCADA monitoring and control interface provides a comprehensive visualization of the gas turbine subsystems, enabling real-time tracking of critical operating variables, supervisory control, data logging at an appropriate sampling rate for performance analysis and fault detection.

Figure 7 presents the normalized measurements during a representative operating transition, showing the coordinated evolution of control signals, pressures, mass flow, power, and turbine-related temperatures. The response rates and staged changes visible in these signals provide information for tuning the model's transient behavior. Nevertheless, agreement with the measured off-design responses does not, by itself, guarantee that the model will imitate the turbine's baseline nominal performance as evaluated at ISO ambient conditions and the reference fuel heating value.

The calibration and validation procedures, including the measurement period, sensor accuracy, and data pre-processing, follow the methodology established by Chaibakhsh and Amirkhani for gas turbine performance modeling [9]. Their framework defines how archived records are screened and how model parameters are tuned against measured data using an optimization-based

Proof Read

procedure. The same approach was adopted here to account for transient operating states, including startup, shutdown, and part-load operation.

3. Mass Flow Calculation

The air intake duct dynamic pressure drop (Δp_{intake}) is parameterized directly as a function of the variable inlet guide vane (IGV) position (Figure 8). Since the compressor inlet mass flow rate scales linearly with the IGV opening degree within its operational envelope ($70 \leq \theta_{IGV} \leq 100$ percent), a linearized intake loss formulation is adopted:

Air intake duct pressure: $$p_{intake} = p_{amb.} - \Delta p_{filters} \tag{3}$$

Pressure drop via filters: $$\Delta p_{filters} = \Delta p_{base} + \Delta p_{span} \left(\frac{\theta_{IGV} - \theta_{min}}{\theta_{max} - \theta_{min}} \right) \tag{4}$$

where θ_{min}=70 and θ_{max} =100. The calibrated parameters (Δp_{base} =0.34 kPa and Δp_{span} =0.8 kPa) yield an exceptional match with real plant DCS measurements across the entire loading range, avoiding unnecessary algebraic complexity while maintaining high physical accuracy.

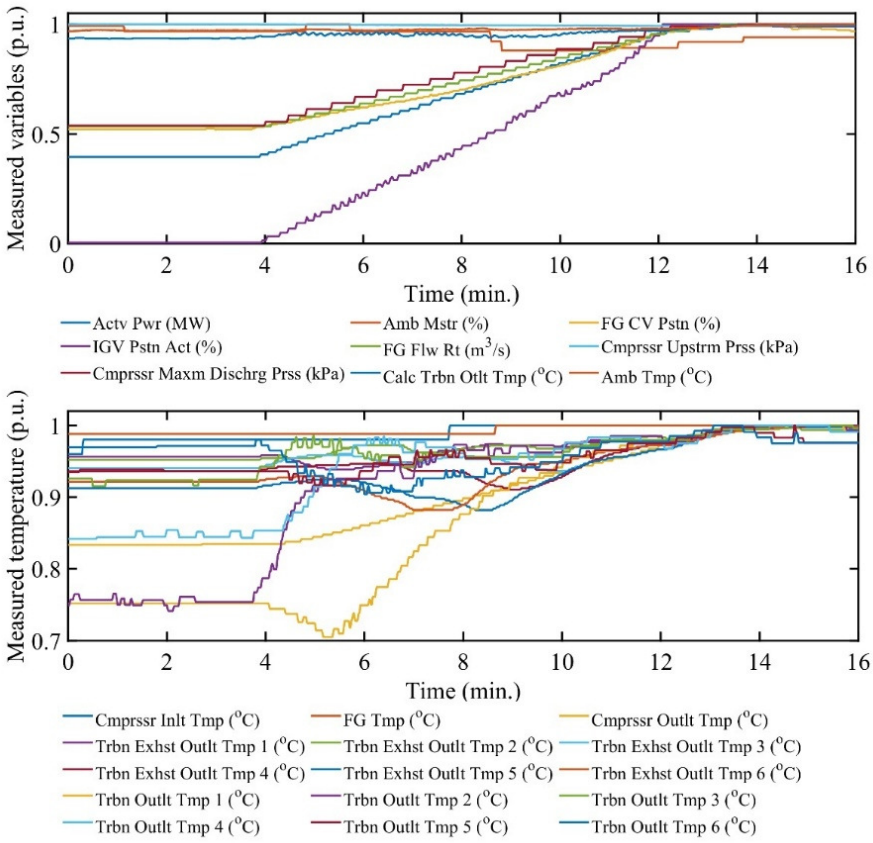


Figure 7. Measured variables for calibrating the gas turbine model

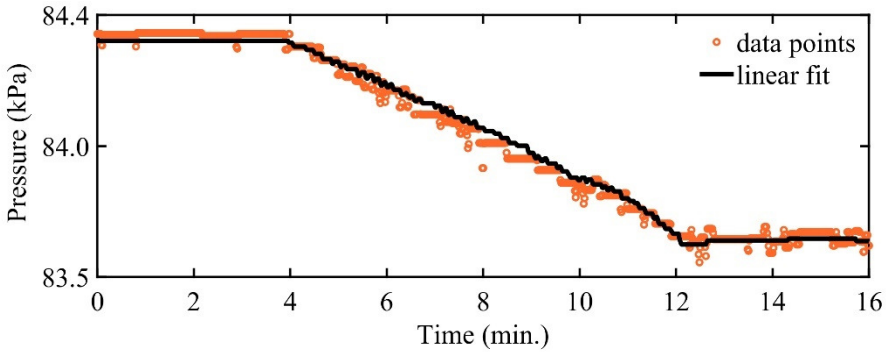


Figure 8. Available measured variables during transient and steady-state conditions

It should be noted that the upgraded version of this heavy-duty gas turbine, MGT-70(3), yields an approximate 10 percent increase in nominal power output compared to its baseline generation, primarily driven by enhanced core mass flow capacity. Consequently, local aerodynamic velocities increase, elevating the characteristic Mach number to approximately M ≈0.45. Under this condition, fluid compressibility effects become significant (density variations exceed ~10 %), meaning that the standard incompressible flow assumption (M<0.3) is no longer valid. [17].

For usability and traceability of the governing computational equations, standard ideal-gas subsonic compressible relations are incorporated as dynamic correction factors. This modification rigorously accounts for density variations while preserving the consistency of the analytical framework. To account for compressibility effects, the ratio of stagnation pressure (p_{intake}) to static pressure ($p_{comp.in}$) is defined as a function of the Mach number (M) using the following isentropic relation:

Subsonic inlet static pressure:
$$\frac{p_{comp.in}}{p_{intake}} = \left(1+\frac{\gamma-1}{2}M^{2}\right)^{-\frac{\gamma}{\gamma-1}}, \quad p_{intake} = p_{amb.} - \Delta p_{filters} \tag{5}$$

The compressor inlet density can be also captured as function of the local density ρ_{air} and M using the following correction relation,

Subsonic density correction:
$$\frac{\rho_{comp.in}}{\rho_{air}} = \left(1+\frac{\gamma-1}{2}M^{2}\right)^{-\frac{1}{\gamma-1}} \tag{6}$$

By adopting the governing equations for the compressor section from Reference [9], the mass flow rate can be estimated as follows,

Air flow rate:
$$\dot{m}_{comp} = (\chi_0 + k_0.\chi.e^{-L_{igv}s})\,\dot{m}_{comp.corr} \tag{7}$$

Corrected air flow rate:
$$\dot{m}_{comp,corr} = \delta_{comp.}\left(\frac{K_{comp}}{\tau_{comp.flow}\,s+1}\right)\left(\frac{p_{comp.dis}-p_{comp.in}}{T_{comp.in}\,\rho_{comp.in}}\right)^{\frac{1}{2}} \tag{8}$$

Correction factor:
$$\delta_{comp.} = \left(\frac{\eta_{comp}}{\eta_{comp.N}}\right)\left(\frac{T_{iso}}{T_{comp.in}}\right)\left(\frac{p_{comp.in}}{p_{iso}}\right)\left(\frac{\omega}{\omega_N}\right) \tag{9}$$

Proof Read

Compressor pressure ratio: $$CPR = \left(\frac{k_1 e^{-L_{cpr} s} \Gamma^{a_1}}{\tau_{comp.cpr} s + 1} \right) \left(\frac{T_{iso}}{T_{comp.in}} \right) \quad , \quad \Gamma = \frac{\dot{W}_{comp}}{\omega_{comp}} \tag{10}$$

4. The Performance and Output Relations

The compressor discharge temperature, the turbine exhaust temperature, and the compressor/turbine efficiencies and power terms constitute the three governing quantities of the gas turbine cycle. The compressor outlet temperature directly determines the cycle's thermal efficiency margin and sets the enthalpy level of the cooling and combustion air, while the turbine outlet temperature represents the exhaust gas energy entering the heat recovery steam generator (HRSG). In combined-cycle operation, even a minor deviation in exhaust temperature significantly affects steam production and HRSG output; thus, accurate off-design prediction of this parameter is vital for evaluating overall plant performance. Based on references [9, 18], the following relationships are obtained:

Compressor efficiency: $$\eta_{comp} = \left(\frac{k_2 \, CPR^{\,a_2} e^{-b_2 \times CPR}}{\tau_{comp.eff} \, s + 1} \right) \left(\frac{T_{iso}}{T_{comp.in}} \right)^{\frac{1}{2}} \tag{11}$$

Turbine efficiency: $$\eta_{turb} = \left(\frac{\eta_{turb0}}{\tau_{turb.eff} \, s + 1} \right) \left(\frac{\omega}{\omega_N} \right) \tag{12}$$

Furthermore, the compressor discharge temperature ($T_{comp.dis}$) and the turbine outlet temperature ($T_{turb.out}$) can be determined given the inlet temperature, pressure ratio, and isentropic efficiencies (η_{comp} and η_{turb}), as follows:

Compressor outlet temp.: $$T_{comp.dis} = T_{comp.in} \left(1 + \frac{1}{\eta_{comp}} \left(\left(\frac{p_{comp.dis}}{p_{comp.in}} \right)^{\frac{\gamma-1}{\gamma}} - 1 \right) \right) \tag{13}$$

Turbine outlet temp. : $$T_{turb.out} = \left(\frac{T_{turb.in}}{\tau_{turb.out} \, s + 1} \right) \left(1 - \eta_{turb} \left(1 - \left(\frac{p_{turb.out}}{p_{turb.in}} \right)^{\frac{\gamma-1}{\gamma}} \right) \right) \tag{14}$$

Accordingly, the mechanical power consumed by the compressor section and the power generated by turbine section can be estimated by following relations,

Compressor power: $$\dot{W}_{comp} = \left(\frac{\dot{m}_{comp.dis} \, C_p(T_{comp.dis}) T_{comp.dis} - \dot{m}_{comp.corr} C_p(T_{comp.in}) T_{comp.in}}{\tau_{comp.pwr} \, s + 1} \right) \tag{15}$$

Turbine power : $$\dot{W}_{turb} = \left(\frac{\dot{m}_{turb.in} \, C_p(T_{turb.in}) \, T_{turb.in} - \dot{m}_{turb.exhst} C_p(T_{turb.exhst}) \, T_{turb.exhst}}{\tau_{turb.gen} \, s + 1} \right) \tag{16}$$

Proof Read

In the next section, based on the established gas turbine performance relations and the developed simulation model, comprehensive correction factor functions are systematically extracted under various environmental and operational conditions.

5. Correction Factors

In this section, four key environmental and operational factors, namely relative humidity, barometric pressure, compressor inlet temperature, and fuel characteristics (*LHV* and *H/C* ratio), which directly influence the air mass flow and power output of the gas turbine, are analyzed and their governing mathematical correlations are extracted. Accordingly, the correction factors for generated power, mass flow rate, efficiency, and exhaust temperature of the gas turbine are calculated and presented.

Ambient relative humidity changes the specific heat capacity (c_p), and density of the working fluid, and alters the compressor aerodynamic work and thermodynamic expansion in the gas turbine. As shown in Figure 9, the reference point where the power correction factor equals unity (P^*=1.0) is established at 60 percent relative humidity, which is consistent with standard ISO conditions. Off-design humidity levels produce temperature-dependent deviations that are most pronounced at subzero and low ambient temperatures, with a decrease around 2.5 percent at -10°C. To separate these psychrometric changes from the intrinsic turbine health parameters within the digital twin framework, cycle simulations were performed at off-design boundaries to parameterize the humidity correction curves.

In Figure 9, power correction factor (P^*) as a function of relative humidity across various ambient temperature is presented. The empirical polynomial coefficients (a_3, b_3 and c_3) associated with Eq. (17) are summarized in Table 2, allowing the power correction factor (P^*) to be calculated across various ambient temperature conditions.

Correction Factor: $$P^* = a_3 x^2 + b_3 x + c_3 \quad (17)$$

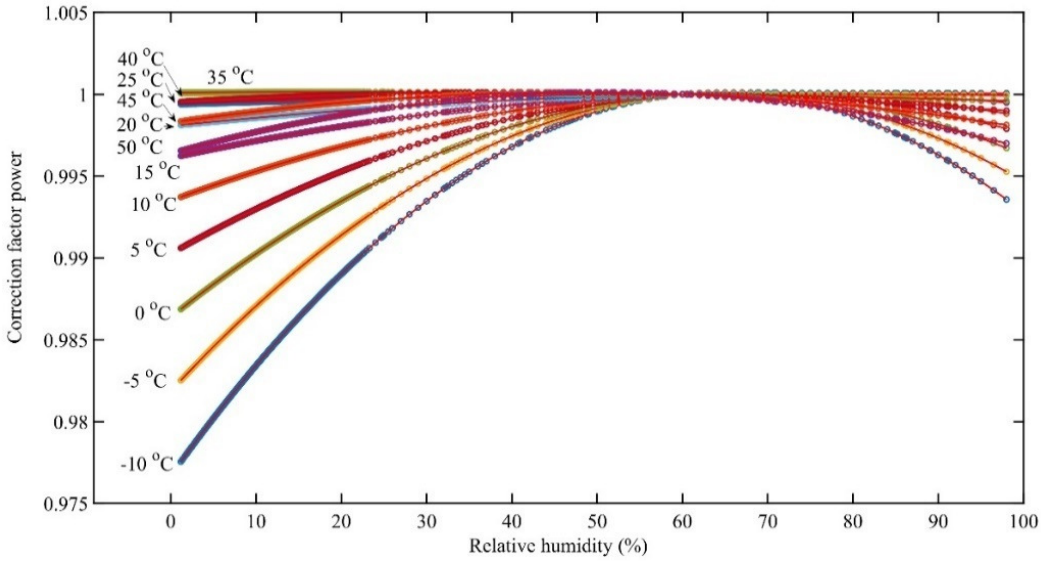


Figure 9. Power correction factor (P^*) as a function of relative humidity across various ambient temperature

Table 2. Polynomial coefficients for power correction factor (P*) as a function of relative humidity at various ambient temperatures

Temp. (°C)	$a_3 \times 10^{-6}$	$b_3 \times 10^{-5}$	c_3	P^* at RH = 0 %	P^* at RH = 60 %	P^* at RH = 100 %
-10	-5.689	72.97	0.9767	0.9767	1.00	0.9928
-5	-4.356	56.37	0.9819	0.9819	1.00	0.9947
0	-3.200	41.9	0.9864	0.9864	1.00	0.9963
5	-2.222	29.57	0.9903	0.9864	1.00	0.9977
10	-1.422	19.37	0.9935	0.9935	1.00	0.9987
15	-8	11.3	0.9961	0.9961	1.00	0.9994
20	-0.3556	5.367	0.9981	0.9981	1.00	0.9999
25	-0.09	1.567	0.9994	0.9994	1.00	1.00
30	0	-0.1	1.00	1.00	1.00	0.9999
35	-0.09	0.366	1.00	1.00	1.00	0.9995
40	-0.3556	2.967	0.9995	0.9995	1.00	0.9989
45	-0.08	7.7	0.9983	0.9983	1.00	0.9980
50	–1.422	14.57	0.9964	0.9964	1.00	0.9968

Figure 10 presents the correction factors for power output (P^*), air mass flow (M^*), thermal efficiency (E^*), and turbine outlet temperature (T^*) as a function of compressor inlet pressure loss (Δp_{in}). As it is illustrated in Figure 10 and expressed by Eq. (18) with the corresponding coefficients given in Table 3, compressor inlet pressure losses (Δp_{in}) exert a severe, compounding penalty on the gas turbine's thermodynamic performance.

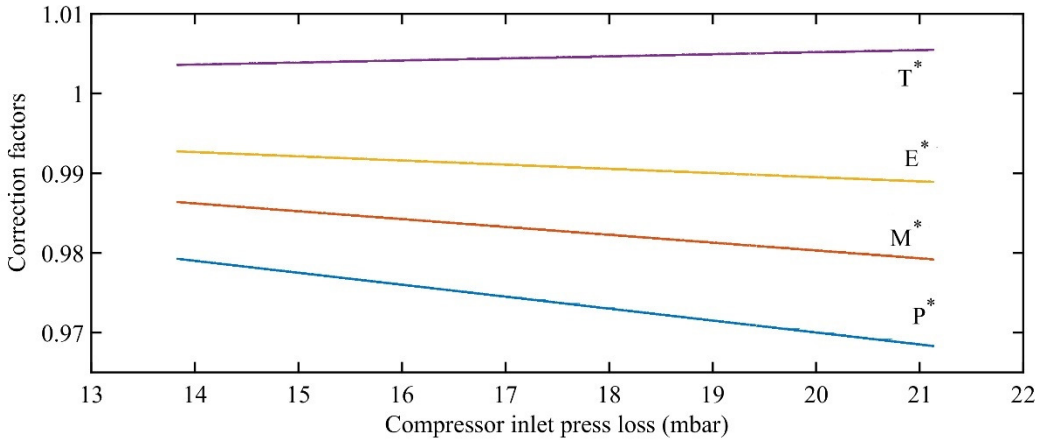


Figure 10. Correction factors for power output (P^*), air mass flow (M^*), thermal efficiency (E^*), and turbine outlet temperature (T^*) as a function of compressor inlet pressure loss (Δp_{in})

Table 3. Performance correction factors under site inlet pressure loss range

Performance parameter	Parameter a_4	Correction at minimum drop Δp_{in} = 13.8 mbar	Correction at mean site drop Δp_{in} = 18.5 mbar	Correction at maximum drop ΔP_{in} = 21.1 mbar	Equivalent degradation relative to ISO
Power Output (P^*)	-0.0015	0.9793	0.9723	0.9683	2.07 ~ 3.17 % loss
Air Mass Flow (M^*)	-0.000985	0.9864	0.9818	0.9792	1.36 ~ 2.08 % reduction
Efficiency (E^*)	-0.000525	0.9928	0.9903	0.9889	0.72 ~ 1.11 % drop
Turbine Outlet Temp. (T^*)	0.00026	1.0036	1.0048	1.0055	0.36 ~ 0.55 % increase

Given the high-altitude site conditions, where ambient barometric pressure is substantially below standard ISO conditions, the baseline air density and mass flow are inherently suppressed. Combined with realistic operational pressure losses ranging from 13.8 to 21.1 mbar, these inlet degradations directly drive down the effective air mass flow (M^*) and thermal efficiency (E^*), culminating in an aggregate power derating (P^*) of up to 3.17 percent. This critical sensitivity explains why annual generated power under these severe site constraints consistently remains below 80 percent of the nominal capacity, underscoring the vital necessity of accounting for inlet pressure corrections in performance monitoring and control optimization.

Correction Factors: $$f(\Delta p_{in}) = 1 + a_4 \times \Delta p_{in} \tag{18}$$

In Figure 11, the correction factors for power output (P^*), thermal efficiency (E^*), air mass flow (M^*), and turbine outlet temperature (T^*) as a function of compressor inlet temperature are presented. As demonstrated in Figure 11 and quantified via the piece-wise quadratic correlations in Table 4 (Eq. 19), the compressor inlet temperature (T_{in}) critically dictates the overall gas turbine performance. These operational constraints are associated with the corrected outlet temperature (OTC), rather than an explicitly imposed mechanical power limit. The OTC can be calculated as follows [11, 19],

$$OTC = \psi(T_{exh}, T_{in}) = \bar{T}_{exh} - (k_1 + k_3 \times T_{in}) \times T_{in} - k_2 \times \left(1 - \frac{\omega}{\omega_N}\right) \tag{19}$$

in which, k_1=0.37, k_2=200 °C and k_3=0.007 °C^{-1} Under the site's low barometric pressure, the control system reduces the IGV opening to prevent the OTC from falling below its allowable operating boundary (512 °C), thereby restricting the air flow and further power increase. Accordingly, this threshold is treated in the model as an operational limit.

Different from conventional expectations, where lower temperatures continuously enhance output, the activation of this operational limits bounds the maximum power and efficiency, resulting in a distinct shift in the regression slope (highlighted by the shaded region) to protect the shaft line and generator from over-torque and mechanical overload.

Correction Factors : $$f(T_{in}) = a_5 \times T_{in}^2 + b_5 \times T_{in} + c_5 \tag{20}$$

Finally, the fuel quality correction factors are presented in Eq. (21). Precise determination of the exact fuel quality entering the turbine remains challenging. This difficulty arises from frequent fuel switching between natural gas and liquid fuel (gasoil), as well as property variations in gasoil procured from diverse sources, stored in large-capacity tanks, and thoroughly blended.

Correction Factor : $$P^* = a_6 \times LHV + b_6 \tag{21}$$

Based on the manufacturer's technical manuals and gas turbine performance tests, the governing correlations have been established using the worst-case fuel quality and the highest national fuel LHV limits, as summarized in Table 5.

Proof Read

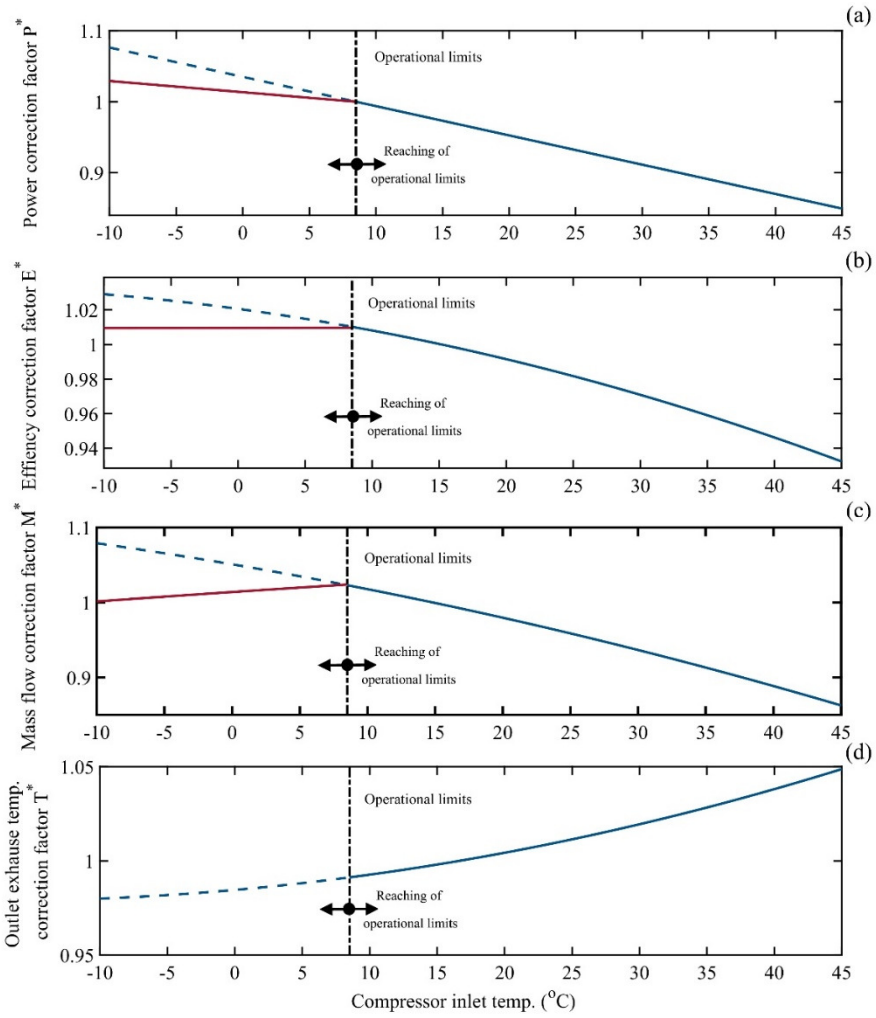


Figure 11. Performance correction factors versus compressor inlet temperature

From a thermodynamic perspective, burning a fuel with a lower *LHV* requires an increased fuel mass flow rate to maintain the required turbine inlet temperature (*TIT*), which increases the total working fluid mass flow expanding through the turbine. Furthermore, lower H/C ratios enhance flame luminosity and radiative heat transfer within the combustor, while altering the specific heat ratio (γ) and heat capacity (c_p) of the flue gas. These effects may contribute to a small increase in power output.

Furthermore, given that the nominal air-to-fuel mass ratio (*A/F*) remains approximately within the range of 50 to 52, variations in fuel composition can significantly disrupt the *A/F*. Consequently, to maintain the required firing temperature and power output, fuel consumption must be adjusted, which in turn alters the effective air mass flow requirements. The corresponding correction factor for mass flow (*M**) and its governing parameters are formulated in Eq. (22) and detailed in Table 6. So, we have,

$$\text{Correction Factor :} \qquad M^{*} = a_7 \times LHV^{2} + b_7 \times LHV + c_7 \tag{22}$$

Table 4. Performance correction factors under compressor inlet temperature variation

Performance parameter	Temp. range	a_5	b_5	c_5
P*	8.5 <=	-	-0.004128	1.035119
	< 8.5	-	-0.001578	1.013443
E*	8.5 <=	-2.019×10^{-5}	-0.0010483	1.0205
	< 8.5	3.24×10^{-7}	9.50×10^{-6}	1.0095
M*	8.5 <=	-2.49×10^{-5}	-0.003067	1.051
	< 8.5	-4.771×10^{-6}	0.00121	1.014
T*	-	1.756×10^{-5}	0.0006349	0.9846

Table 5. Fuel correction factor parameters and coefficients based on LHV and H/C ratios

Hydrogen to Carbon ratio *(H/C)*	a_6	b_6	Correction Factor at Worst Quality (*LHV* = 41.0 MJ/kg)	Correction Factor at Best Quality (*LHV* = 48.594 MJ/kg)
2.9	−0.001087	1.05433	1.0098	1.0015
3.150	−0.001103	1.05262	1.0074	0.9990
3.300	−0.001121	1.05125	1.0053	0.9968
3.450	−0.001109	1.04883	1.0033	0.9949

Table 6. Mass flow rate correction parameters

Performance parameter	a_7	b_7	c_7
M*	1.273×10^{-5}	-0.001592	1.048

Finally, the overall corrected performance metrics, including power output (*P**), air mass flow (*M**), thermal efficiency (*E**), and turbine outlet temperature (*T**), are determined by applying the relevant correction factors for compressor inlet temperature (T_{in}), relative humidity (*RH*), compressor inlet pressure loss (ΔP_{in}), and fuel lower heating value (*LHV*). For each performance metric X, the total correction factor is calculated as,

$$\text{Correction Factor Total:} \quad X^*_{total} = X^*_{Temp.} \times X^*_{RH} \times X^*_{\Delta p} \times X^*_{LHV} \tag{23}$$

This allows rapidly computing off-design performance states under varying ambient gradients without relying on heavy iterative cycle solvers.

6. Conclusion

This study developed a performance model for the SGT5-2000E / MGT-70(3) gas turbine and correction functions for key environmental and operational variables, including humidity, barometric pressure, compressor inlet temperature, and fuel properties. While operational charts typically cover the turbine's full operating range, this study used one year of performance data, site-specific air pressure, and a digital-twin model to regenerate them for the turbine's actual operating envelope. The resulting charts estimate power output, air mass flow, thermal efficiency, and exhaust temperature under site conditions. The analysis also considered inlet pressure losses, fuel-quality variations, and mechanical constraints at low compressor inlet temperatures. The

Proof Read

model supports performance assessment under conditions not represented by standard ISO ratings. Conventional correction charts remain useful because they are simple and practical, but they are limited to predefined variables and do not continuously assess a turbine's changing condition. Integrating physics-based digital twins directly with SCADA and condition-monitoring systems can enable online performance assessment under varying operating conditions and, with validated diagnostic methods, fault detection, progression assessment, and remaining-useful-life estimation.

In this framework, correction charts should serve as references for model development and validation, not as the main tool for operators to interpret correction factors or apply derived formulas manually. Future work should integrate the present correction framework into a validated digital-twin architecture and evaluate it using continuous, full-scale operational data to support timely maintenance decisions and reduce operating cost.

Disclosure statement

No potential conflict of interest was reported by the author(s).

Notes on contributors



Amirreza Mostafavi received the B.Sc. degree in mechanical engineering from the University of Guilan, Rasht, Iran, in 2021. He is currently an M.Sc. student in mechanical engineering at the University of Guilan. Since 2020, he has been a research assistant and a member of the Intelligent Systems and Advanced Control Laboratory at the University of Guilan. He has been working at MAPNA Power Services Company since 2026. His research interests include fault diagnosis and fault prognosis of industrial gas turbines.



Farzad Farokhi is an Instrumentation and Control (I&C) Engineer at MAPNA Group, currently serving as the Power Plant Manager of the Goharan Sirjan Combined Cycle Power Plant at MAPNA Power Plant Service Company. He holds an M.Sc. in Electrical Engineering, specializing in Electronics, from Iran University of Science and Technology (IUST). Since 2010, he has served as a key member of the company, with expertise in Power Plant Control Systems, particularly Distributed Control Systems (DCS).



Ali Chaibakhsh is a Professor of Mechanical Engineering at the University of Guilan, bringing a broad academic and industrial background in process control and instrumentation. He received his B.Sc. degree from the University of Guilan in 2002, and subsequently earned his M.Sc. and Ph.D. in Mechanical Engineering from K.N. Toosi University of Technology, Tehran, in 2004 and 2009, respectively. His research focuses on the design and application of intelligent systems in condition monitoring, fault diagnosis, and fault prognosis, aiming to enhance operational efficiency, reliability, and automation capabilities.

Proof Read

References

[1] Y. Zhang, P. Liu, and Z. Li, "Gas turbine off-design behavior modelling and operation windows analysis under different ambient conditions," *Energy,* vol. 262, p. 125348, 2023/01/01/ 2023, doi: https://doi.org/10.1016/j.energy.2022.125348.

[2] S. Sanaye and S. Hosseini, "Off-design performance improvement of twin-shaft gas turbine by variable geometry turbine and compressor besides fuel control," *Proceedings of the Institution of Mechanical Engineers, Part A: Journal of Power and Energy,* vol. 234, no. 7, pp. 957-980, 2020/11/01 2020, doi: 10.1177/0957650919887888.

[3] H. O. Egware and A. I. Obanor, "The investigation of an SGT5-2000E gas turbine power plant performance in Benin City based on energy analysis," *Energy Conversion and Management: X,* vol. 16, p. 100316, 2022/12/01/ 2022, doi: https://doi.org/10.1016/j.ecmx.2022.100316.

[4] A. T. Ekechi, "Conceptual framework for process optimization in gas turbine performance and energy efficiency," *International Journal of Multidisciplinary Futuristic Development,* 2020.

[5] J. Kurzke, "Model Based Gas Turbine Parameter Corrections," 2003. [Online]. Available: https://doi.org/10.1115/GT2003-38234.

[6] X. Hu and M. Yan, "Data Assimilation for Online Calibration of Simulation Digital Twin - A Case Study with Multiple Model Parameters," 2024/1/1/: IEEE, 2024, pp. 2844-2855, doi: 10.1109/WSC63780.2024.10838855. [Online]. Available: https://doi.org/10.1109/WSC63780.2024.10838855

[7] Z. Jiang, X. Wang, S. Yang, J. Liu, and H. Chen, "Representation of Components Characteristics under Performance Degradation of Gas Turbine Engine," 2022/1/1/, vol. 2: American Society of Mechanical Engineers, 2022, doi: 10.1115/GT2022-83001. [Online]. Available: https://doi.org/10.1115/GT2022-83001

[8] P. A. Gardner, M. Dal Borgo, V. Ruffini, Y. Zhu, and D. J. Wagg, "Towards the Development of an Operational Digital Twin," *Vibration,* vol. 3, no. 3, pp. 235-265, 2020/9/1/ 2020, doi: 10.3390/vibration3030018.

[9] A. Chaibakhsh and S. Amirkhani, "A simulation model for transient behaviour of heavy-duty gas turbines," *Appl. Therm. Eng.,* vol. 132, pp. 115-127, 3/5/ 2018, doi: https://doi.org/10.1016/j.applthermaleng.2017.12.077.

[10] *SGT5-2000E Heavy-Duty Gas Turbine (50 Hz): Technical Specifications and Product Overview*, Siemens Energy AG, Munich, Germany, 2024. [Online]. Available: https://www.siemens-energy.com/global/en/home/products-services/product/sgt5-2000e.html.

[11] *MGT-70(3) Gas Turbine: Technical Data and Product Specification*, MAPNA Turbine Engineering Manufacturing, Tehran, Iran, 2022.

[12] A. Shahrabi Farahani, H. Kohandel, H. Moradtabrizi, S. Khosravi, E. Mohammadi, and A. Ramesh, "Power generation gas turbine performance enhancement in hot ambient temperature conditions through axial compressor design optimization," *Applied Thermal Engineering,* vol. 236, p. 121733, 2024/01/05/ 2024, doi: https://doi.org/10.1016/j.applthermaleng.2023.121733.

[13] H. Hanachi, J. Liu, A. Banerjee, and Y. Chen, "Effects of Humidity Condensation on the Trend of Gas Turbine Performance Deterioration," *Journal of Engineering for Gas Turbines and Power,* vol. 137, no. 12, 2015, doi: 10.1115/1.4030815.

[14] R. Kurz and K. Brun, "Degradation in gas turbine systems," *J. Eng. Gas Turbines Power,* vol. 123, no. 1, pp. 70-77, 2001.

[15] *Gas turbines - Acceptance tests*, International Organization for Standardization, Geneva, Switzerland, 2009. [Online]. Available: https://www.iso.org/standard/43118.html.

[16] D. Orhon and P. Ropiteau, "Development of User Gas Turbine Performance Calculation Tool Based on the ASME PTC 22 Code," in *Turbo Expo*, 2025, vol. 88834: American Society of Mechanical Engineers, p. V007T19A009.

[17] M. R. Pakatchian and H. Saeidi, "A practical axial compressor design optimization approach based on gas turbine operation," 2019/1/1/: Avestia Publishing, 2019, doi: 10.11159/ffhmt19.131. [Online]. Available: https://doi.org/10.11159/ffhmt19.131

[18] A. Mostafavi and A. Chaibakhsh, "Dynamic physics-based digital twin for supervisory, condition monitoring and fault diagnosis of industrial turboshaft engines," *Digital Twin,* vol. 3, no. 2, p. 2598085, 2026/04/03 2026, doi: http://doi:10.1080/27525783.2025.2598085.

Proof Read

[19] MAPNA-Group, "Gas Turbine Performance / Acceptance Test Specification for V94.2 (5)/ MGT-70 (2): Parehsar Combined Cycle Power Plant Project," MAPNA Group, Iran, , 2009.

ProofRead